Perspective Photometric Stereo with Shadows*

Roberto Mecca, Guy Rosman, Ron Kimmel, and Alfred M. Bruckstein

Technion - Israel Institute of Technology,
Department of Computer Science

Abstract. High resolution reconstruction of 3D surfaces from images remains an active area of research since most of the methods in use are based on practical assumptions that limit their applicability. Furthermore, an additional complication in all active illumination 3D reconstruction methods is the presence of shadows, whose presence cause loss of information in the image data. We present an approach for the reconstruction of surfaces via Photometric Stereo, based on the perspective formulation of the Shape from Shading problem, solved via partial differential equations. Unlike many photometric stereo solvers that use computationally costly variational methods or a two-step approach, we use a novel, well-posed, differential formulation of the problem that enables us to solve a first order partial differential equation directly via an alternating directions raster scanning scheme. The resulting formulation enables surface computation for very large images and allows reconstruction in the presence of shadows.

Keywords: Photometric Stereo, Perspective Shape from Shading, Shadows, up-wind scheme, semi-Lagrangian scheme.

1 Introduction

The classical computer vision topic of Shape from Shading (SfS) was recently revitalized by a series of research contributions driven in part by some interesting new applications [1–3]. The technique based on the shape recovery from several pictures of the same scene taken under different illuminations, namely Photometric Stereo (PS), has gained some popularity, due to the feasibility of implementing controlled light systems. In this context, quite a few multi-image depth recovery techniques based on inverting shading models have been addressed in the literature [4, 5]. Utilizing multiple images in order to remove both the nonlinearities in the image irradiance equation and the generally unknown albedo, new ideas have been introduced in order to solve the PS problems more efficiently, see [6–9].

Most of the works which addressed the PS problem, for example [1, 5, 10, 11], reconstruct the surface in two steps:

* This research was partly supported by European Community's FP7- ERC program, grant agreement no. 267414 and by Broadcom foundation.

A. Kuijper et al. (Eds.): SSVM 2013, LNCS 7893, pp. 258–269, 2013.

1. the estimation of the gradient of the surface (usually via some local minimization algorithms);
2. the recovery of the height from the gradient field all over the domain (by integration or by functional minimization).

In the framework of classical PDEs for a single input image and known albedo there exists a well known direct approach to SfS which uses level sets [12]. Its drawback, among others, is the need to know a-priori the albedo, which limits the scope of applications where this method can be employed. Here, we present a new model for a direct recovery of the surface considering Perspective Photometric Stereo with n images (PPS_n) with shadows. In Section 2 we recall the differential formulation for the PPS_2 introduced in [9] with only two images. Section 3 contains the construction of the proposed differential problem taking into account multiple images containing shadows. Note that our hypotheses are weaker than the ones assumed in [4] which addressed the same problem without the perspective transformation and considered a two step procedure with regularization terms for smooth surfaces. We will focus here on a surface recovery based on the direct computation of the unique weak (Lipschitz) solution of a linear PDEs.

The theoretical formulation of the new differential approach can be easily extended when more than three images are considered. The mathematical proof of the existence and uniqueness of a weak solution for this new formulation is sketched in Section 4. The numerical schemes are presented in Section 5 where both up-wind and semi-Lagrangian methods are implemented considering the *Fast Sweeping* technique. In Section 6 we show some numerical tests in order to demonstrate the order of consistency of the numerical schemes and the fast reconstruction of the surface respectively. In particular, in these tests we consider images of several megapixels with a significant portion of shadow areas. Section 7 concludes the paper.

2 Perspective Photometric Stereo Technique

In this section we briefly recall the model for the PSfS, and the direct solution method described for this case, as presented in [9]. Let us define the observed surface as $h(x, y) = (x, y, \hat{z}(x, y))$. We define a far light source by its unit vector ω. The associated reflectance equation is given by the Lambertian illumination model [13]:

$$I = \rho(\omega \cdot n), \quad \omega = (\omega_1, \omega_2, \omega_3), \quad \omega_3 < 0 \tag{1}$$

where ρ is the unknown albedo function, I is the image and n is the incoming unit normal to the surface. There are several ways to describe the perspective transformation of the surface [1, 2, 14]. Here we consider the one introduced in [15], based on the following transformation

$$k(\xi, \eta) = (\xi, \eta, z(\xi, \eta)) = \Big(-\frac{x}{\hat{z}(x, y)} f, -\frac{y}{\hat{z}(x, y)} f, \hat{z}(x, y) \Big) \tag{2}$$

where $\hat{z}(x,y) = z(\xi,\eta)$ and the positive quantity f is the focal length and the point (ξ,η) belongs to the perspective domain in the focal plane (in blue in Fig. 1), namely $\overline{\Omega}^p = \Omega^p \cup \partial\Omega^p$.

The differential formulation for the PSfS problem

$$\rho(\xi,\eta)\frac{-fz_\xi\omega_1 - fz_\eta\omega_2 - (z+\xi z_\xi+\eta z_\eta)\omega_3}{\sqrt{f^2(z_\xi^2+z_\eta^2)+(z+\xi z_\xi+\eta z_\eta)^2}} = I(\xi,\eta), \quad \text{for} \quad (\xi,\eta)\in\Omega^p \tag{3}$$

is not well-posed even if the Dirichlet boundary condition, i.e. $z(\xi,\eta) = g(\xi,\eta)$ is given [15].

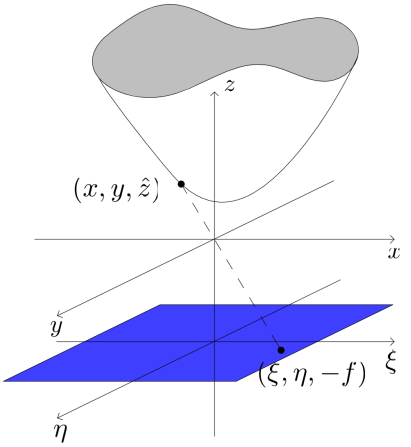

Fig. 1. Schematic representation of a surface taken under perspective view. The point of the real surface $(x,y,\hat{z})$ is projected in the perspective domain in the point (ξ,η) of the focal plane (in blue), parallel to the optical one (xy-plane) at a focal distance f.

In [9] the classical PS technique has been modified to a well posed formulation of the PPS_2 problem involving surface recovery via a direct differential approach. Two light sources given by ω' and ω'' are considered resulting in the following non-linear system of PDEs,

$$\begin{cases} \rho(\xi,\eta)\dfrac{-z_\xi(f\omega_1'+\xi\omega_3')-z_\eta(f\omega_2'+\eta\omega_3')-z\omega_3'}{\sqrt{f^2(z_\xi^2+z_\eta^2)+(z+\xi z_\xi+\eta z_\eta)^2}} = I_1(\xi,\eta), & \text{on } \Omega^p \\ \rho(\xi,\eta)\dfrac{-z_\xi(f\omega_1''+\xi\omega_3'')-z_\eta(f\omega_2''+\eta\omega_3'')-z\omega_3''}{\sqrt{f^2(z_\xi^2+z_\eta^2)+(z+\xi z_\xi+\eta z_\eta)^2}} = I_2(\xi,\eta), & \text{on } \Omega^p \\ z(\xi,\eta) = g(\xi,\eta) & \text{on } \partial\Omega^p. \end{cases} \tag{4}$$

Simplifying the common quantity $\frac{\rho(\xi,\eta)}{\sqrt{f^2(z_\xi^2+z_\eta^2)+(z+\xi z_\xi+\eta z_\eta)^2}}$, the system can be written as the following well-posed problem,

$$\begin{cases} b(\xi,\eta)\cdot\nabla z(\xi,\eta) + s(\xi,\eta)z(\xi,\eta) = 0, & \text{on } \Omega^p \\ z(\xi,\eta) = g(\xi,\eta) & \text{on } \partial\Omega^p \end{cases} \tag{5}$$

where

$$b(\xi,\eta) = \begin{pmatrix} (f\omega_1' + \xi\omega_3')I_2(\xi,\eta) - (f\omega_1'' + \xi\omega_3'')I_1(\xi,\eta) \\ (f\omega_2' + \eta\omega_3')I_2(\xi,\eta) - (f\omega_2'' + \eta\omega_3'')I_1(\xi,\eta)) \end{pmatrix} \tag{6}$$

and

$$s(\xi,\eta) = \omega_3' I_2(\xi,\eta) - \omega_3'' I_1(\xi,\eta). \tag{7}$$

We recall that (5) admits only one weak (i.e. Lipschitz) solution, under the main assumptions that are the absence of shadows and the knowledge of the Dirichlet boundary condition $g(\xi,\eta)$. To overcome these limitations in real applications we consider the PSfS problem with more than two images as the basic model. In this case, an additional potential advantage beyond computational efficiency is the possible noise robustness of the direct method. Furthermore, we exploit the extra image data not only to address noise – but rather to allow reconstruction in the presence of shadows. In the numerical tests we shall demonstrate that significant portions of the image can be missing (see the black patches in Fig. 3) without impeding the correct surface recovery.

3 Direct Surface Reconstruction Using Multiple Images and Shadows

We now generalize the model shown in Section 2 for more than two images. We start with 3 images, which is the minimal number of images that allow a computation of the boundary condition without a-priori knowing the albedo [11]. We start by writing the PDEs (5) resulting from each image pair

$$\begin{cases} b^{(1,2)}(\xi,\eta)\cdot\nabla z(\xi,\eta) + s^{(1,2)}(\xi,\eta)z(\xi,\eta) = 0, & \text{a.e. } (\xi,\eta)\in\Omega^p \\ b^{(1,3)}(\xi,\eta)\cdot\nabla z(\xi,\eta) + s^{(1,3)}(\xi,\eta)z(\xi,\eta) = 0, & \text{a.e. } (\xi,\eta)\in\Omega^p \\ b^{(2,3)}(\xi,\eta)\cdot\nabla z(\xi,\eta) + s^{(2,3)}(\xi,\eta)z(\xi,\eta) = 0, & \text{a.e. } (\xi,\eta)\in\Omega^p \end{cases} \tag{8}$$

where

$$b^{(h,k)}(\xi,\eta) = \begin{pmatrix} (f\omega_1^h + \xi\omega_3^h)I_k(\xi,\eta) - (f\omega_1^k + \xi\omega_3^k)I_h(\xi,\eta) \\ (f\omega_2^h + \eta\omega_3^h)I_k(\xi,\eta) - (f\omega_2^k + \eta\omega_3^k)I_h(\xi,\eta) \end{pmatrix} \tag{9}$$

and

$$s(\xi,\eta)^{(h,k)} = I_k(\xi,\eta)\omega_3^h - I_h(\xi,\eta)\omega_3^k. \tag{10}$$

A similar formulation has been given in [11], however in that paper the authors propose a two step procedure, computing explicitly the partial derivatives in the perspective variables (ξ,η). In other words, they do not treat the system (8) as a PDE system, but rather as a linear system, where the unknowns i.e. the entries of ∇z (namely $p = \frac{\partial z}{\partial \xi}$ and $q = \frac{\partial z}{\partial \eta}$), are computed *locally*.

Let us start by taking into account the differential formulation (8). We exploit the linearity of the hyperbolic equations in (8) by simply summing them, resulting in the single differential equation

$$\begin{cases} \left(b^{(1,2)} + b^{(1,3)} + b^{(2,3)}\right)\cdot\nabla z(\xi,\eta) + \left(s^{(1,2)} + s^{(1,3)} + s^{(2,3)}\right)z(\xi,\eta) = 0 \\ z(\xi,\eta) = g(\xi,\eta). \end{cases} \tag{11}$$

It is clear that, since the solution of each equation in (8) is the same (i.e. the differential problem (5) has a unique solution [9]), the problem (11) will be also satisfied by the same solution. However, a proof of uniqueness can not be obtained as a consequence of this sum. In fact, it is easy to prove that by subtracting some terms instead of summing all the addends, the problem becomes ill-posed. That is why we shall prove the existence of a unique weak solution for a problem such as (11) which also takes into account shadows and occlusions. In order to have a well-posed problem the boundary condition $g(\xi, \eta)$ is needed which can be readily obtained using the three available images and a two step procedure applied only on the boundary pixels assuming no occlusions on $\partial\Omega^p$.

Note that, if more than three images are available, we can easily generalize this reasoning. In the general case, defining the functions

$$b_n(\xi,\eta) = \sum_{r\in\binom{[n]}{2}} b^r(\xi,\eta) \quad \text{and} \quad s_n(\xi,\eta) = \sum_{r\in\binom{[n]}{2}} s^r(\xi,\eta) \tag{12}$$

the extension of the PDE-based approach for the PPS_n problem can be readily stated as

$$\begin{cases} b_n(\xi,\eta)\cdot\nabla z(\xi,\eta) + s_n(\xi,\eta)z(\xi,\eta) = 0, \text{ a.e. } (\xi,\eta)\in\Omega^p \\ z(\xi,\eta) = g(\xi,\eta) \qquad\qquad\qquad\qquad\qquad \forall(\xi,\eta)\in\partial\Omega^p \end{cases} \tag{13}$$

where with $\binom{[n]}{2}$ we call the set that contains the couple of integer indexes with no repetition. For example, if $n = 3$ we have $\binom{[n]}{2} = \{(1,2),(1,3),(2,3)\}$.

3.1 Weighted Perspective Photometric Stereo for Multiple Images with Shadows

The main idea of this paper is based on the possibility of ensuring the well-posedness of the PPS_n problem formulation (13) by exploiting the linearity of the operation involved in the basic differential formulation (5). It is also clear that (5) still does not lose the well-posedness if we multiply both sides (i.e. $b(\xi,\eta)$ and $s(\xi,\eta)$) by a function $q(\xi,\eta)$. That is:

$$\begin{cases} q(\xi,\eta)b(\xi,\eta)\cdot\nabla z(\xi,\eta) + q(\xi,\eta)s(\xi,\eta)z(\xi,\eta) = 0 \\ z(\xi,\eta) = g(\xi,\eta) \end{cases} \tag{14}$$

still has a unique Lipschitz solution. We do not go deeper with the discussion on the weak regularity of q. Here, we merely consider it as a smooth function.

We are now able to define the weighted PPS_n equation (W-PPS_n) by replacing b_n, s_n in (12) with

$$b_n^w(\xi,\eta) = \sum_{r\in\binom{[n]}{2}} q_r(\xi,\eta)b^r(\xi,\eta) \quad \text{and} \quad s_n^w(\xi,\eta) = \sum_{r\in\binom{[n]}{2}} q_r(\xi,\eta)s^r(\xi,\eta) \tag{15}$$

where the index r is used here only to make clear that we are now considering $\binom{n}{2}$ continuous functions.

We have now completed the set-up of the W-PPS$_n$ formulation with

$$\begin{cases} b_n^w(\xi,\eta)\cdot\nabla z(\xi,\eta) + s_n^w(\xi,\eta)z(\xi,\eta) = 0, \text{ a.e. } (\xi,\eta)\in\Omega^p \\ z(\xi,\eta) = g(\xi,\eta) \qquad\qquad\qquad\qquad \forall(\xi,\eta)\in\partial\Omega^p. \end{cases} \tag{16}$$

We will explain in the next part how shadows will influence the definition of the vector field b_n^w and the scalar field s_n^w.

A key point is the possibility to use weights q_r that are not only positive. It is possible to maintain the well-posedness of the problem also by considering non-negative weights q_r that vanish at some points for some image pairs.

It can be shown that for the set of well-posed differential equations, maintaining a non-negative weight for at least one image pair suffices to give us a well-posed problem.

This allows us to adapt the W-PPS$_n$ equations for the case of shadows in some of the images. Specifically, let $\mathcal{S}^r$ define the areas that are shaded in either of the images in pair r. We define $\widetilde{q}_r$ as the indicator function,

$$\widetilde{q}_r(\xi,\eta) = \mathbb{1}_{[\overline{\Omega}^p\setminus\mathcal{S}^r]}(\xi,\eta). \tag{17}$$

In other words we consider the weights as switches able to locally put out go the global sums in (15) the functions b_r and s_r that do not contain relevant information due to the presence of shadows in the involved images. Finally we construct the weights q_r as smooth cutoff functions based on $\widetilde{q}_r$.

4 Uniqueness of the Weak Solution of W-PPS$_3$

In order to complete the theoretical analysis we will extend the uniqueness results of the differential problem (16) in the case of a weak solution. Discussion of depth-discontinuities and multiple objects is beyond the scope of this paper. Our purpose is to prove the uniqueness of solution of (16) in the Lipschitz function space via characteristics method. The meaning of weak solution here is intended as combination of classical solutions, each defined on a different domain. These domains are then going to be patched together in such a way that, across the boundaries between domains on which there are discontinuities in some derivatives, the equation (16) is satisfied. Let us recall that the points where the surface z is not differentiable are the same where the functions b_n^w and s_n^w are discontinuous (jump discontinuity) [8]. We assume the discontinuity points as the family of regular curves $(\gamma_1(t),\ldots,\gamma_k(t))$ where t is the argument of the parametric representation.

A complete proof of the well-posedness of our model can be given in a manner similar to [16]. It is based on the following two features of our model:

1. the absence of critical points for the projected characteristic field, i.e. $b_3^w(\xi,\eta)\neq(0,0)$;
2. the propagation of the information from the boundary is not prevented between two sets separated by discontinuity curves $(\gamma_1(t),\ldots,\gamma_k(t))$, see Fig. 2.

The following result is very important since it guarantees the absence of critical points that would prevent the method to work.

Lemma 1. *Assume that* $\bigcap_r \mathcal{S}^r = \emptyset$. *Then* $|b_3^w(\xi,\eta)| \neq 0$, $\forall(\xi,\eta) \in \Omega^p$.

This last result is not only important for the proof of uniqueness of weak solution. We use it also for the well-posedness of the numerical schemes introduced in Section 5.

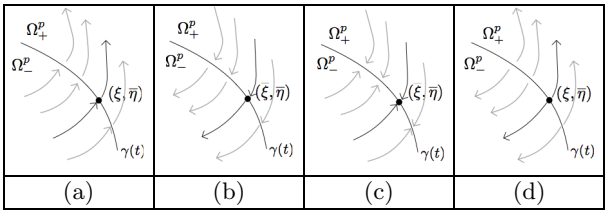

Fig. 2. Among the four possibilities shown for b_3^w, only the cases (a) and (b) allow the information to cross the discontinuity curve γ without needing additional data as required in (c) and (d)

The next results ensure that the characteristic method can actually be applied since the discontinuity on $\gamma(t)$ is not an obstacle for propagating a solution of the PDE.

Theorem 1. *Let* $\gamma(t)$ *be a regular curve of discontinuity for the function* $b_3^w(\xi,\eta)$ *(and* $s_3^w(\xi,\eta)$*) and let* $(\overline{\xi},\overline{\eta})$ *be a point along* $\gamma(t)$. *Let* $n(\overline{\xi},\overline{\eta})$ *be the outgoing normal with respect to the set* Ω^p_+, *then we have*

$$\left[\lim_{\substack{(\xi,\eta)\to(\overline{\xi},\overline{\eta})\\(\xi,\eta)\in\Omega^p_+}} b_3^w(\xi,\eta)\cdot n(\overline{\xi},\overline{\eta})\right]\left[\lim_{\substack{(\xi,\eta)\to(\overline{\xi},\overline{\eta})\\(\xi,\eta)\in\Omega^p_-}} b_3^w(\xi,\eta)\cdot n(\overline{\xi},\overline{\eta})\right] \geq 0 \qquad (18)$$

The result that permits to prove the uniqueness of weak solution is readily proved now. With Lemma 1 and Theorem 1 it is possible to show that the uniqueness can be reached using the characteristic strip method. In order to understand the idea behind the proofs of Lemma 1 and Theorem 1 we refer to [16] where the same results are proved in the case with only two images.

We emphasize once more the advantages of this new formulation with respect to [11]. The first is obviously the direct computation of the height of the surface, without passing through the preliminary computation of the partial derivatives. This would result in a slower computation of the 3D surface and also needs the condition that the 3D surface has to be smooth. That is the surface should be at least C^1. The second and much more important point is that, since our W-PPS$_3$ model is based on the differential problem (5) for two images (which admits a unique Lipschitz solution), even if we have three images with disjoint shadows we can still reconstruct the surface.

5 Numerical Schemes

Next, we consider the numerical methods used to obtain the solution. The difference among those presented in [9] and our is related to the different implementation. It allows to speed up the convergence of the four numerical schemes we will discuss in the following sections. The algorithms we implemented use the *fast sweeping* technique [17–20] which exploits the regularity of the vector field b_3^w.

For the numerical schemes we consider the domain $\overline{\Omega}^p = [a^p, b^p] \times [c^p, d^p] = [-1, 1]^2$ with a uniform discretization space step $\Delta_\xi = (b^p - a^p)/n$ and $\Delta_\eta = (c^p - d^p)/m$ where n and m are the number of intervals divide the sides of the rectangular domain (that is $\xi_i = a^p + i\Delta_\xi$, $\eta_j = c^p + j\Delta_\eta$ with $i = 0, \ldots, n$ and $j = 0, \ldots, m$). We will denote by $\overline{\Omega}_d^p$ all the points of the lattice belonging to $\overline{\Omega}^p$, by Ω_d^p all the internal points and by $\partial\Omega_d^p$ all the boundary points.

5.1 Forward Numerical Schemes

We want to recall now the numerical schemes used for the forward approximation of (16) where the propagation of the information is considered starting from the inflow part of the boundary

$$\Gamma_{in} = \left\{ (\widetilde{\xi}, \widetilde{\eta}) \in \partial\Omega^p : \nu(\widetilde{\xi}, \widetilde{\eta}) \cdot \lim_{\substack{(\xi.\eta)\to(\widetilde{\xi},\widetilde{\eta}) \\ (\xi,\eta)\in\Omega^p}} b_3^w(\xi, \eta) \leq 0 \right\} \tag{19}$$

where $\nu(\xi, \eta)$ represents the outgoing normal to the boundary $\partial\Omega^p$. It is clear that in the previous definition the limit is taken since it can happen that a discontinuity curve can coincide with the boundary. Now we can formulate the differential problem solved by the forward schemes as follow:

$$\begin{cases} b_3^w(\xi, \eta) \cdot \nabla z(\xi, \eta) + s_3^w(\xi, \eta) z(\xi, \eta) = 0, \text{ a.e. } (\xi, \eta) \in \Omega^p \\ z(\xi, \eta) = g(\xi, \eta) \qquad\qquad \forall (\xi, \eta) \in \Gamma_{in}. \end{cases} \tag{20}$$

In order to simplify the notation we will call $b_3^w(\xi_i, \eta_j)$ as $b_{i,j} = (b_{i,j}^1, b_{i,j}^2)$ and $s_3^w(\xi_i, \eta_j)$ as $s_{i,j}$.

Forward Up-Wind Scheme:

$$Z_{i,j}^F = \frac{\Delta_\eta |b_{i,j}^1| Z_{i-\mathrm{sgn}(b_{i,j}^1),j}^F + \Delta_\xi |b_{i,j}^2| Z_{i,j-\mathrm{sgn}(b_{i,j}^2)}^F}{|b_{i,j}^1|\Delta_\eta + |b_{i,j}^2|\Delta_\xi + \Delta_\xi \Delta_\eta s_{i,j}}. \tag{21}$$

In our case the numerical schemes are applied to digital images where clearly $\Delta_\xi = \Delta_\eta = \Delta$.

Forward Semi-Lagrangian Scheme:

$$z_{i,j}^F = z^F(\xi_i - h\alpha_{i,j}^1, \eta_j - h\alpha_{i,j}^2) \frac{|b_{i,j}|}{|b_{i,j}| + h s_{i,j}} \tag{22}$$

where $\alpha_{i,j} = \frac{b_{i,j}}{|b_{i,j}|}$ and the parameter $h > 0$ is assumed equal to the size of the grid Δ in order to reach the highest order of convergence equal to one ([9]).

5.2 Backward Numerical Schemes

The backward numerical schemes are based on the approximation of the surface propagating the information stored on the outflow part of the boundary

$$\Gamma_{out} = \partial\Omega^p \setminus \Gamma_{in}. \tag{23}$$

The formulation of these schemes can be easily obtained considering the following equivalent problem

$$\begin{cases} -b_3^w(\xi,\eta)\cdot\nabla z(\xi,\eta) - s_3^w(\xi,\eta)z(\xi,\eta) = 0, \text{ a.e. } (\xi,\eta)\in\Omega^p \\ z(\xi,\eta) = g(\xi,\eta) \qquad\qquad\qquad\qquad \forall(\xi,\eta)\in\Gamma_{out} \end{cases} \tag{24}$$

and repeating always the same passages for the forward ones.

Backward Up-Wind Scheme:

$$Z^B_{i,j} = \frac{\Delta_\eta |b^1_{i,j}| Z^B_{i+\mathrm{sgn}(b^1_{i,j}),j} + \Delta_\xi |b^2_{i,j}| Z^B_{i,j+\mathrm{sgn}(b^2_{i,j})}}{|b^1_{i,j}|\Delta_\eta + |b^2_{i,j}|\Delta_\xi + \Delta_\xi\Delta_\eta s_{i,j}}. \tag{25}$$

Backward Semi-Lagrangian Scheme:

$$z^B_{i,j} = z^B(\xi_i + h\alpha^1_{i,j}, \eta_j + h\alpha^2_{i,j})\frac{|b_{i,j}|}{|b_{i,j}| - hs_{i,j}}. \tag{26}$$

Let us emphasize that, in order to have all these schemes well defined, we have to take the parameter Δ (equal to h) small enough to have:

$$\begin{aligned} |b^1_{i,j}| + |b^2_{i,j}| + \Delta s_{i,j} \neq 0 \quad & \text{for both forward and backward u-w schemes} \\ |b_{i,j}| + hs_{i,j} \neq 0 \quad & \text{for the forward s-L scheme} \\ |b_{i,j}| - hs_{i,j} \neq 0 \quad & \text{for the backward s-L scheme} \end{aligned} \tag{27}$$

always possible since $|b_3^w(\xi,\eta)| \neq 0$, $\forall(\xi,\eta)\in\Omega^p$, Lemma 1 ([9]). Due to lack of space it is not possible to give theoretical results regarding these numerical schemes. An exhaustive discussion about the consistency, proof of convergences and estimation of the error with perturbed data, can be found in [16] where the case with only two images is taken into account.

6 Numerical Tests

We now present several results of our method. We will consider the W-PPS$_3$ problem with some *artificial shadow* regions defined in the images. The smooth surface v_{reg} exhibits three high slopes. The second one v_{lip} is a Lipschitz surface with a very high Lipschitz constant (i.e. the gradient changes sharply its direction across the point where the surface is not differentiable). Note also that the boundary condition is not constant for either of them. In particular, v_{lip} has a boundary condition differentiable almost everywhere. As mentioned at the

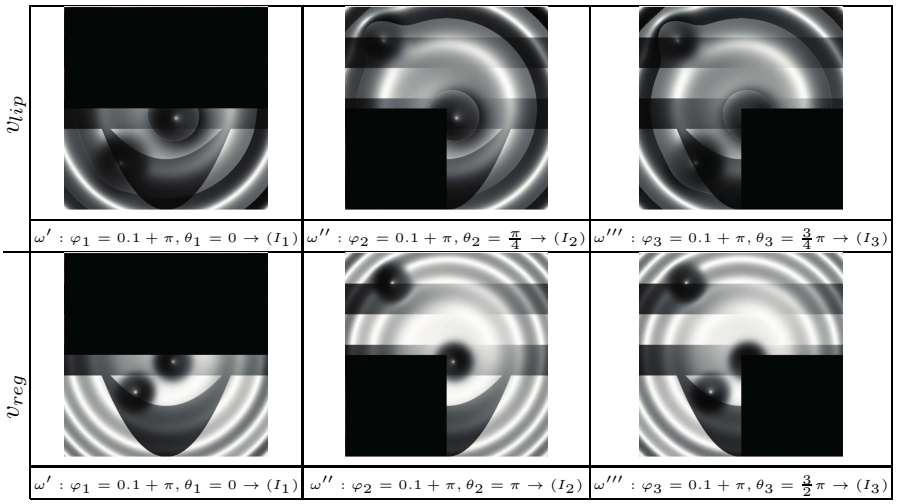

Fig. 3. Set of images used with the respective light sources described by their spherical coordinates. In this case the albedo mask and Gaussian noise (10%) is added for all the images.

beginning of the paper, well-posedness holds even if the albedo is not known. In order to exploit this advantage of our model we consider the initial images shown in Fig. 3. In order to reconstruct the surface in the worst situation we set artificial shadows for which the union of the shadow sets almost completely covers the image domain. In Fig. 3 are shown the starting data, images and light sources directions, used in the numerical tests.

Table 1. The values of this table explain how (in precision and in time) the semi-Lagrangian and the up-wind schemes converge for the v_{lip} case

v_{lip}		Forward schemes				Backward schemes			
	Δ	L^∞ s-L	time (sec)	L^∞ u-w	time (sec)	L^∞ s-L	time (sec)	L^∞ u-w	time (sec)
10 %	500	1.552×10^{-1}	0.259	2.613×10^{-1}	0.500	1.586×10^{-1}	0.026	3.014×10^{-1}	0.023
	1000	9.586×10^{-2}	1.313	1.651×10^{-1}	2.257	9.968×10^{-2}	0.135	1.818×10^{-1}	0.078
	2000	5.956×10^{-2}	5.676	1.020×10^{-1}	8.314	6.068×10^{-2}	0.483	1.090×10^{-1}	0.338
	4000	3.957×10^{-2}	21.372	6.366×10^{-2}	32.089	3.856×10^{-2}	1.650	6.650×10^{-2}	1.247
	500	1.980×10^{-1}	0.273	2.650×10^{-1}	0.492	2.587×10^{-1}	0.031	3.065×10^{-1}	0.021
	1000	1.247×10^{-1}	1.516	1.832×10^{-1}	2.431	1.237×10^{-1}	0.109	2.001×10^{-1}	0.080
	2000	8.742×10^{-2}	5.601	1.127×10^{-1}	8.786	8.805×10^{-2}	0.418	1.194×10^{-1}	0.325
	4000	9.098×10^{-2}	21.687	1.127×10^{-1}	8.786	9.080×10^{-2}	1.642	1.024×10^{-1}	1.258

The size of the images take into account varies from 500×500 pixels (with $\Delta = 0.004$) to 4000×4000 pixels, that is 16 megapixels (for a spacial step $\Delta = 0.0005$). The running times quoted are for a 2.4 Ghz Core i5 computer with 8 GB (1333Mhz) of RAM. Tables 1 and 2 show that the convergence of the schemes is not prevented by the presence of noise even if the consistency order is not even one like for the images without noise. The computational time is very small even for the largest size images. The difference between the forward and

Table 2. The values of this table explain how (in precision and in time) the semi-Lagrangian and the up-wind schemes converge for the v_{reg} case

v_{reg}		Forward schemes				Backward schemes			
	Δ	L^∞ s-L	time (sec)	L^∞ u-w	time (sec)	L^∞ s-L	time (sec)	L^∞ u-w	time (sec)
10 %	500	6.152×10^{-2}	0.077	1.916×10^{-1}	0.062	6.152×10^{-2}	0.031	2.671×10^{-1}	0.019
	1000	3.237×10^{-2}	0.319	1.263×10^{-1}	0.252	3.234×10^{-2}	0.104	1.390×10^{-1}	0.098
	2000	1.672×10^{-2}	1.416	8.065×10^{-2}	1.098	1.671×10^{-2}	0.415	8.167×10^{-2}	0.331
	4000	8.518×10^{-3}	5.024	5.141×10^{-2}	3.954	8.515×10^{-3}	1.642	5.178×10^{-2}	1.233
	500	1.019×10^{-1}	0.077	2.186×10^{-1}	0.156	1.024×10^{-1}	0.026	2.395×10^{-1}	0.019
	1000	1.303×10^{-1}	0.324	1.894×10^{-1}	0.737	1.299×10^{-1}	0.103	1.913×10^{-1}	0.106
	2000	1.048×10^{-1}	1.462	1.193×10^{-1}	3.681	1.052×10^{-1}	0.492	1.202×10^{-1}	0.327
	4000	4.698×10^{-2}	5.096	7.186×10^{-2}	16.935	4.691×10^{-2}	1.649	7.228×10^{-2}	1.255

the backward time of convergences is due to the direction of the vector field b_3^w which results for both cases much more easy passable from the backward than the forward.

Fig. 4 demonstrates the results obtained with the semi-Lagrangian and up-wind fast-sweeping approach.

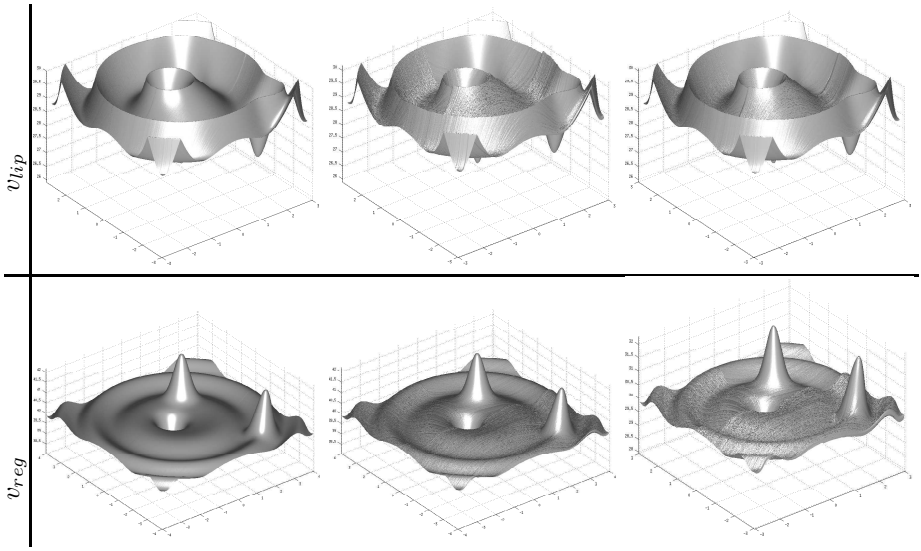

Fig. 4. Left-to-right: groundtruth surface, reconstruction via the semi-Lagrangian scheme, reconstruction via the up-wind scheme

7 Conclusion and Perspective

In this paper we have presented a new direct method for Photometric Stereo in the case of perspective viewing geometry in the case of multiple images and shadows. Using a fast-sweeping update, we are able to update the solution along characteristic lines in an efficient an accurate manner. The resulting algorithm is highly parallelizable and efficient to compute also on a single CPU, and seems promising for real-time implementation.

References

1. Wu, C., Narasimhan, S.G., Jaramaz, B.: A multi-image shape-from-shading framework for near-lighting perspective endoscopes. IJCV, 211–228 (2009)
2. Deguchi, K., Okatani, T.: Shape reconstruction from an endoscope image shape-from-shading technique for a point light source at the projection center. In: Workshop on MMBIA, pp. 290–298. IEEE Computer Society (1996)
3. Yeung, S.Y., Tsui, H.T., Yim, A.: Global shape from shading for an endoscope image. In: Taylor, C., Colchester, A. (eds.) MICCAI 1999. LNCS, vol. 1679, pp. 318–327. Springer, Heidelberg (1999)
4. Hernández, C., Vogiatzis, G., Cipolla, R.: Shadows in three-source photometric stereo. In: Forsyth, D., Torr, P., Zisserman, A. (eds.) ECCV 2008, Part I. LNCS, vol. 5302, pp. 290–303. Springer, Heidelberg (2008)
5. Onn, R., Bruckstein, A.M.: Integrability Disambiguates Surface Recovery in Two-Image Photometric Stereo. IJCV 5, 105–113 (1990)
6. Lee, S., Brady, M.: Integrating stereo and photometric stereo to monitor the development of glaucoma. Image and Vision Computing 9, 39–44 (1991)
7. Mecca, R.: Uniqueness for shape from shading via photometric stereo technique. In: ICIP, pp. 2933–2936 (2011)
8. Mecca, R., Falcone, M.: Uniqueness and approximation of a photometric shape-from-shading model. Accepted to SIAM Journal on Imaging Sciences (2012)
9. Mecca, R., Tankus, A., Bruckstein, A.M.: Two-Image Perspective Photometric Stereo Using Shape-from-Shading. In: Lee, K.M., Matsushita, Y., Rehg, J.M., Hu, Z. (eds.) ACCV 2012, Part IV. LNCS, vol. 7727, pp. 110–121. Springer, Heidelberg (2013)
10. Kimmel, R., Yavneh, I.: An algebraic multigrid approach for image analysis. SIAM Journal on Scientific Computing 24, 1218–1231 (2003)
11. Tankus, A., Kiryati, N.: Photometric stereo under perspective projection. In: ICCV, pp. 611–616 (2005)
12. Kimmel, R., Bruckstein, A.M.: Tracking level sets by level sets: A method for solving the shape from shading problem. CVIU 62, 47–58 (1995)
13. Horn, B.K.P., Brooks, M.J.: Shape from Shading. The MIT Press (1989)
14. Prados, E., Faugeras, O.D.: Shape from shading: A well-posed problem? In: CVPR, vol. 2, pp. 870–877. IEEE Computer Society (2005)
15. Tankus, A., Sochen, N.A., Yeshurun, Y.: Shape-from-shading under perspective projection. IJCV 63, 21–43 (2005)
16. R.Mecca, Tankus, A., Bruckstein, A.: Two-image perspective photometric stereo: Analytical and numerical analysis of a new differential model. Technical report, Technion - Israel Institute of Technology, Computer Science Department (2013)
17. Danielsson, P.E.: Euclidean distance mapping. Computer Graphics And image Processing 14, 227–248 (1980)
18. Qian, J., Zhang, Y.T., Zhao, H.K.: Fast sweeping methods for eikonal equations on triangular meshes. SIAM J. Numer. Anal. 45, 83–107 (2007)
19. Weber, O., Devir, Y.S., Bronstein, A.M., Bronstein, M.M., Kimmel, R.: Parallel algorithms for approximation of distance maps on parametric surfaces. ACM Trans. Graph. 27, 104:1–104:16 (2008)
20. Chacon, A., Vladimirsky, A.: Fast two-scale methods for eikonal equations. SIAM J. Scientific Computing 34 (2012)